Monitoring and scheduling of pollution disaster in agricultural waters based on INSAR

Yijun Liu[a], Ziwen Zhang[a,*], Yang Li[b], Tie Liu[c], Wujian Ye[a], Shaowei Weng[b]

[a]School of Information Engineering, Guangdong University of Technology, Guangzhou, 510006, China,
emails: yunkm2258@126.com (Y. Liu), zhzw2018@163.com (Z. Zhang)
[b]Graduate School of integrated basic science, Nihon University, Tokyo, 156-8550, Japan
[c]Xinjiang Institute of Ecology and Geography, Chinese Academy of Sciences, Urumqi, 830011, China

ABSTRACT

Objective: To improve the quality of monitoring image in agricultural waters by effective methods, to obtain information of the pollution disaster in agricultural waters in time, to provide the necessary data for the disaster management and decision making of agricultural waters, and to promote the development of agricultural economy in this region.
Methods: by using the monitoring and scheduling method for pollution disaster in agricultural waters based on INSAR, comprehensive and accurate monitoring of pollution disaster in agricultural waters can be conducted. SRTM3 DEM is used to eliminate baseline error in INSAR interferogram. According to different scattering characteristics of different ground objects in the INSAR image, the gray value is different, and a two-dimensional gray histogram is built to preprocess the INSAR image so as to avoid the false alarm in the detection of the edge of the agricultural waters. Through the monitoring method of ground wave spectrum, the two directions reflection ratio factor of waterbody is measured, and the correlation between the pollution of agricultural waters and the ground spectrum is studied, and the monitoring and scheduling of the pollution disaster in the agricultural waters are effectively carried out.
Results: there is a significant correlation between the pollution in agricultural waters and the satellite reflectance spectrum on the ground, with a correlation coefficient of about 0.8. The false area which is not connected with the agricultural waters of the preprocessed INSAR image is almost completely removed by using the proposed method. The boundary of the extracted water area is well matched with the boundary of the actual image. The false alarm rate and the leakage rate for processing the agricultural waters image under different scenes are all very low, and the accuracy of the INSAR image extraction and calculation efficiency are better and with good robustness. The proposed method can reduce the strong scattering point and the speckle noise of the building, and effectively restrain the edge of the buildings, such as the buildings around the agricultural waters. The information of disaster change in agricultural waters obtained by the proposed method is relatively accurate.
Conclusion: the proposed method can extract the image of agricultural waters and obtain the information of the pollution disaster in agricultural waters in real time and accurately, so as to realize the effective monitoring and scheduling of the pollution disaster in the agricultural waters.

Keywords: INSAR; Agricultural waters; Monitoring and scheduling of pollution disaster; Two-dimensional gray histogram; Mathematical morphology; Spectral monitoring

* Corresponding author.

1. Introduction

Because of the need of economic development, the development and utilization of agricultural waters is becoming more and more large, which leads to the increasing frequency of red tide, oil spill, dangerous chemicals, and leakage of warm water [1–4]. The occurrence of these disasters is often sudden. It is impossible to predict the time, location, the scope of the contaminated water, the migration path of the pollutants, the intensity of the pollution, and so on. In order to get the relevant information of the disaster as soon as possible and provide the necessary data for the timely and accurate decision of the managers, it is necessary to carry out the emergency monitoring and scheduling of the pollution disaster in the agricultural waters [5–8].

The INSAR technology developed in the last 10 years can detect the water changes in the direction of radar line of sight in real time by mm level precision (altitude), high resolution (*m* level in horizontal direction, 10 m level), and large range (above 100×100 km^2) [9]. The technology has been successful in monitoring the field of large-scale surface deformation, such as seismic deformation and volcanism, and it also shows great superiority in monitoring and scheduling of pollution disaster in agricultural waters. At present, some cities have carried out some experiments and achieved good results. However, the measurement accuracy of INSAR images is affected by many factors, for example, temporal decorrelation reduces the quality of the image phase, the tropospheric delay causes the image distortion, and the satellite orbit error causes the additional fringe in the image. These factors seriously restrict the accuracy of the INSAR image and its further application [10]. Therefore, the research on the monitoring and scheduling of the pollution disaster in agricultural waters based on INSAR is proposed, the INSAR image is optimized in depth, and the related factors of the pollution disaster in the agricultural waters are analyzed.

2. Materials and methods

2.1. Experimental materials

The experiment is carried out in an agricultural demonstration area of a coastal area. The study area is a suburb, surrounded by an industrial production area. There are two chemical plants, one cement plant, and three fuel plants in the industrial production area. During the past years 2000–2010, serious damage has occurred in the area, which poses a threat to the agricultural economy. At present, the hydrological monitoring network and GPS observation point have been set up in the area and the surrounding area, and the monitoring and scheduling network for the pollution disaster in agricultural waters is formed. In this process, the INSAR technology is being applied gradually.

A total of 17 satellite INSAR images from the tested area are obtained, and five pairs of images with interference baseline less than 200 m are selected for optimization. The data error is reduced by using GPS station and merging SRTM3 DEM. SRTM3 DEM is a digital surface elevation model obtained by the space shuttle in the 11 d flight from February 11 to 22, 2000, using radar mapping technology, which covers 80% of the surface waters between 60° north latitude and 54° south latitude. Phase unwrapping

is performed by Goldstein branch cutting to interferometric phase [11]. The horizontal reference is WGS-84 reference ellipsoid, and the vertical datum is the EGM96 geoid of WGS-84. The horizontal resolution of the experimental area is 30 m (1″), the resolution of other regions is 90 m (3″), the absolute height accuracy is 20 m, and the relative elevation accuracy is 16 m. At present, the DEM with 90 m resolution (SRTM3 DEM) is the best choice for monitoring the pollution disaster in global agricultural waters [12].

2.2. Monitoring and scheduling method of pollution disaster in agricultural waters based on INSAR

2.2.1. Reduction of interferogram to tropospheric delay error based on GPS station

Due to the fluctuation of water vapor content in the troposphere, the propagation of radar microwave in the atmosphere will be delayed. The tropospheric delay can cause about 1–10 cm phase delay in interferogram, thus affecting the interpretation and analysis of interferograms. When GPS is used for precise positioning, tropospheric delay is regarded as the error source and noise. In GPS meteorology, these noises are estimated as signals. The 12 GPS stations in the experimental area were built and operated at the end of 2005, and the site distribution is shown in Fig. 1. Based on the continuous observation data of the 12 stations, the coordinate measurement and difference constraints are carried out in seven GPS stations with near distance. The experiment uses the GAMIT software to calculate the time series of the tropospheric delay, and the tropospheric delay parameters are estimated for each 30 min. Fig. 2 gives the time series of zenith total delay (ZTD) for each GPS station in February 2017. It can be seen that the ZTD can reach about 2.34 m, and the change within 1 month can reach about 1 cm. Spatial resolution (station spacing) is usually dozens of km, and GPS is dozens of m. Therefore, it is necessary to interpolate the corrected INSAR interferogram of tropospheric
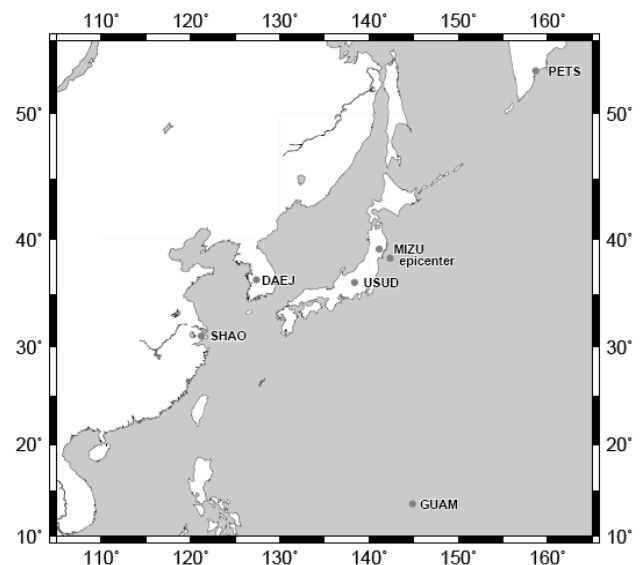

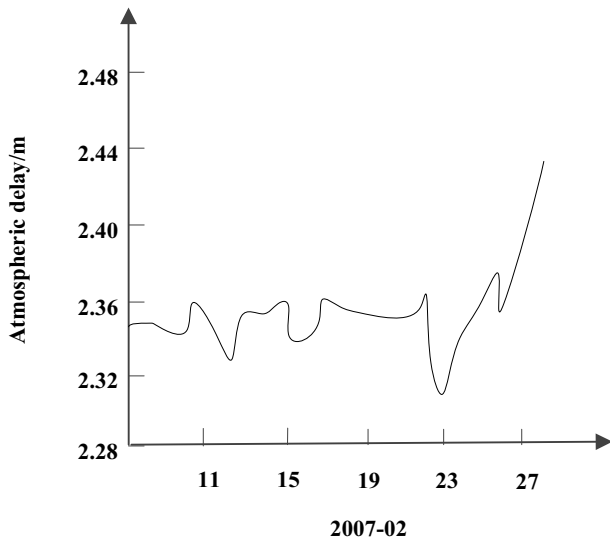Fig. 1. Distribution of INSAR station in experimental area.

Fig. 2. Total zenith tropospheric delay at INSAR station in February 2007.

delay effect in the zenith tropospheric delay obtained by GPS. The results show that the zenith tropospheric delay obtained by the GPS station can improve the low frequency part of the tropospheric delay error, making the residual error of the tropospheric delay less than 5 mm.

2.2.2. Fusion of SRTM3 DEM to eliminate residual baseline error

The error of the satellite orbit determination will be transferred directly to the interference baseline, thus producing obvious additional stripes on the interferogram, which are known as the residual stripe of the ground effect or the baseline error stripe. The baseline error stripe is usually hyperbolic in the INSAR interferogram. If it is not eliminated, it will directly affect the accuracy of the interference measurement, which leads to the wrong interpretation of the pollution disaster in the agricultural waters. According to the expression of the additional stripe in the interferogram, based on the difference result of SRTM3 DEM, the number of stripe of distance and azimuth is calculated by FFT, and then the elimination is carried out [13]. However, this method can only eliminate linear terms, and it is difficult to eliminate the nonlinear baseline error.SRTM3 DEM is used to calculate the nonlinear baseline error surface of the entangled phase by using the method of surface fitting, and it is replaced by the unwrapping phase [14]. This method can not only eliminate the large scope of the baseline error but also eliminate the tropospheric delay error with low frequency signal. SRTM3 DEM is applied to the fitting of the nonlinear baseline error surface, and the unwrapping phase is used to instead.

2.2.3. Construction of 2D gray histogram to preprocess INSAR image

In the process of monitoring and scheduling of the pollution disaster in agricultural waters, it needs to extract INSAR images of waters. In a more complex INSAR image of agricultural waters, there are buildings and other man-made objects besides water. Therefore, the direct application of edge detection operator also requires human judgment whether the detection result is the edge of water or buildings, which is not conducive to the automation of edge detection. Therefore, according to the different scattering characteristics of different ground objects in the INSAR image, the gray value is different, and considering the influence of the speckle noise of the INSAR image, the INSAR image is preprocessed by constructing the two-dimensional gray histogram to suppress the speckle and the edge of the building, so that the false alarm of edge detection for the agricultural waters is avoided [15].

In high-resolution INSAR images, buildings and other man-made objects are mainly composed of bright lines and bright spots. Because of the complex surface structure and special materials, it is easy to form angular reflection or second scattering, the gray scale of the man-made objects in the image is obviously higher than that in other areas. However, due to the smooth surface of the agricultural waters in INSAR images, the echo of the specular reflection is weak, and the dark areas appear in the images. Therefore, it can distinguish the buildings and other man-made objects from agricultural waters by threshold segmentation.

One-dimensional threshold segmentation is a simple method of segmentation. Because the method only considers the gray level of pixels, and does not make use of the correlation and statistical information of pixels and their neighborhood space, the segmentation effect of INSAR images is not ideal [16]. Here, we distinguish the buildings, agricultural waters, and noise by constructing the two-dimensional histogram of INSAR images. The method uses the pixel gray level and the neighborhood mean to express the two-dimensional histogram, while the pixel gray information and the neighborhood spatial gray information of the pixel are considered, and the noise resistance is greatly enhanced.

An image with a gray level of L is set up. The gray value at pixel (a_0, b_0) is $t(a_0, b_0)$, and the average gray value of $Z \times Z$ neighborhood space around this point is $o(a_0, b_0)$. The number of pixels satisfying $t = i$ and $o = j$ is $h(i,j)$, and two-dimensional histogram image $H(t,o)$ is constructed. The two-dimensional gray histogram is as shown in Fig. 3, the two regions on the diagonal line I and II correspond to the background and the target, and the region III and IV far away from the diagonal correspond to the edges and noise.

Fig. 4 is the INSAR image of high-resolution agricultural waters to be treated. It can be seen that there are many buildings, with bright white strong scattering points, which have large-edge intensity in edge detection, causing false alarm.

The 5×5 window is used as the neighborhood of pixels, and the mean value of each pixel neighborhood in the INSAR image of the agricultural water area is calculated. The two-dimensional gray histogram of the agricultural waters is constructed, as shown in Fig. 5. It can be seen that the highlights of the histogram are almost all distributed in a strip near the diagonal line. According to the definition of the histogram, the points outside the strip are edge pixels and noise pixels.

Fig. 6 is a graph segmented by strip and vertical straight line. First, the width c of the strip is determined. The noise
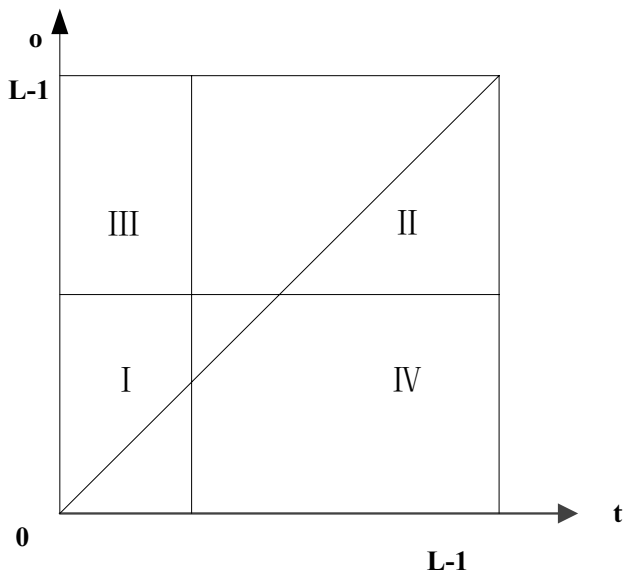
Fig. 3. Two-dimensional gray histogram of agricultural waters.

Fig. 4. High-resolution INSAR image to be processed.

Fig. 5. Two-dimensional gray histogram.

Fig. 6. Strip and vertical straight-line segmentation.

or edge of the pixels near the diagonal area is not obvious, and it has little influence on the subsequent edge detection. The farther away from the histogram diagonal point is, the more obvious the noise is, and the greater the impact on subsequent processing is. In order to suppress the noise better, the stripe width should be as small as possible, but this will increase the computation cost and also lose the image information. By comprehensive consideration, 95% of the total number of points in the strip is as an example to get the strip width c.

In order to get better segmentation and speckle reduction effect, median filter is applied to the pixels outside the stripe. Median filtering is a nonlinear smoothing technique that uses the median of all pixel gray levels in a neighborhood space around a pixel to replace the pixel. While removing the noise, it can retain the edge information of the image [17].

In two-dimensional images, the window of the median filter is square, approximately circular or crisscross. In this case, a square window with a center 5×5 of the pixel point correspondi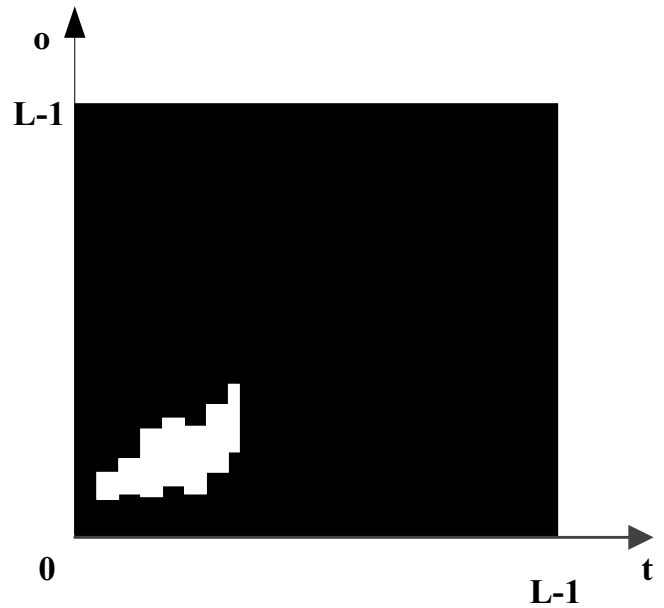ng to a point outside the strip is selected as an example, and the median of the pixels in the window is selected and the median value is used to replace the gray level of the pixel.

After filtering the points outside the strip, the points in the area will approach the diagonal line. Then a vertical line is selected in the strip to segment the image. The linear abscissa μ is the mean value of the gray level of the whole image, and the pixels larger than the threshold are regarded as the man-made objects such as the buildings, to carry out hard limiting processing. The intensity of the strong scattering points can be reduced to decrease the edge strength to prepare for the subsequent processing [18]. Fig. 7 is a preprocessed INSAR

image, which effectively suppresses the strong scattering points and speckle patterns of buildings, and preserves the edge information of agricultural waters.

2.2.4. Enhancing edge features of INSAR image by mathematical morphology

After preprocessing the INSAR image, there are many isolated highlights in the image edge, the edge is broken and the features are not obvious. The edge detection results of INSAR image are further processed by using mathematical morphology operations to remove isolated highlights and enhance the edge characteristics of agricultural waters. Mathematical morphology is widely used in digital image processing. It is used to measure or extract the corresponding shape in the INSAR image with a certain form of structural element to realize the recognition or analysis of the specific target in the image [19]. The basic operations of mathematical morphology operations are expansion and corrosion, which are defined as follows: F is the image to be processed, C is the structural element, and (x,y) is the image coordinate:

$$\text{Expansion: } F + C = \left\{(x,y):C(x,y)\cap F \neq \varphi\right\} \tag{1}$$

$$\text{Corrosion: } F \,!\, C = \left\{(x,y):C(x,y)\subset F\right\} \tag{2}$$

Expansion means that after the structural element C translates (x,y), all points that intersection of C and F is not empty are made to form a set. The corrosion is to transfer the structural element C to (x,y), and C is contained in the set of all points of F. Usually the structure element selects a square array in which the element is 1:

$$C = \begin{bmatrix} 1 & 1 & 1 \\ 1 & 1 & 1 \\ 1 & 1 & 1 \end{bmatrix} \tag{3}$$

Fig. 7. Preprocessed INSAR image.

In this paper, mathematical morphology function bwmorph is used to do mathematical morphology operations on INSAR images to enhance image edge features.

$$\text{BW }2 = \text{bwmorph}\left(\text{BW1},\text{operation},n\right) \tag{4}$$

where the parameter 'Operation' is the morphological operation of INSAR images, including corrosion operation, expansion operation and eliminating solitary highlights, etc. The parameter n is the number of operations to it, and BW1 and BW2 are the set of points after translation. After corrosion of the INSAR image and eliminating burrs, the isolated highlights in the image are removed and the expansion operation is carried out to enhance the edge features.

2.2.5. Monitoring and scheduling of pollution disaster in agricultural waters

Mathematical morphology processing of edge features of INSAR images can effectively extract the edge features of agricultural waters. On this basis, the correlation between the pollution of agricultural waters and the ground spectrum is studied so as to effectively monitor and schedule the pollution disaster of agricultural waters [20]. The following methods are used to verify it.

(i) Method of ground wave spectrum monitoring

Considering the influence of the sun and atmosphere, the bi-directional reflectance factor (BRF) of the water is generally measured in the field. It is obtained by monitoring the radiance of the reflected water and reflecting the radiance of the diffuse body under the same irradiation and observation conditions, and then obtaining the ratio [21].

$$P\left(\sigma_i,\delta_i,\sigma_p,\delta_p\right) = \frac{M_i\left(\sigma_i,\delta_i,\sigma_p,\delta_p\right)}{M_p\left(\sigma_i,\delta_i,\sigma_p,\delta_p\right)} \tag{5}$$

In Eq. (5), $P(\sigma_i, \delta_i, \sigma_p, \delta_p)$ is the BRF of target, $M_i(\sigma_i, \delta_i, \sigma_p, \delta_p)$ is the radiance of target reflection, and $M_p(\sigma_i, \delta_i, \sigma_p, \delta_p)$ is the radiance of the reflected diffuse body.

In actual monitoring, a reflective reference plate is used instead of a fully reflected diffuse body, and a spectral instrument is used to monitor the radiance of the reflection of the water body surface and the radiance of the reflected reference plate under the same irradiation and observation conditions [22]. Considering the linear relationship between the output signal value of the spectrometer and the incident radiant value, Eq. (2) is used to calculate $P(\sigma_i, \delta_i, \sigma_p, \delta_p)$:

$$P\left(\sigma_i,\delta_i,\sigma_p,\delta_p\right) = \frac{N_i\left(\sigma_i,\delta_i\right)}{N_p\left(\sigma_p,\delta_p\right)} f\left(\sigma_i,\delta_i,\sigma_p,\delta_p\right) \tag{6}$$

In Eq. (6), $f(\sigma_i, \delta_i, \sigma_p, \delta_p)$ is the spectral reflection ratio of the reflection reference plate; $N_i(\sigma_i, \delta_i)$ is the signal value of the instrument output when measuring the reflection reference plate; $N_p(\sigma_p, \delta_p)$ is the signal value of the instrument output N when the target is measured.

(ii) A spectral measuring instrument for water body

The reflection of the water body is generally lower than the land target, so it is very important to improve the radiative resolution and the signal-to-noise ratio of the instrument to identify the small spectral reflectance of the agricultural waters. The type VF921 surface spectrometer is an instrument for measuring the spectrum of ground objects developed by a light machine. The instrument uses 256 elements linear array CCD as detector, the wavelength range is 400–1,100 nm, the spectral resolution is 6 nm, and the sensitivity is high. The instrument can work continuously at 3 h, store up to 496 curves, and have interfaces, which can be easily connected with PC to transmit data. In order to make the instrument more suitable for the measurement of low reflection agricultural waters, the instrument has been improved. To detect small radiance changes, the method of increasing gain is adopted, and the increase of signal-to-noise ratio is obtained by increasing integration time [11].

(iii) Calibration of the measuring instrument

Calibration of sensors is a very important aspect to ensure the accuracy and reliability of measurement data. Before and after each measurement, spectral calibration and radiometric calibration are strictly carried out.

3. Results

3.1. Synchronous monitoring results of spectral characteristics

The agricultural waters of a city include three parts of the river water, the reservoir body, and the sewage water body [23]. The spectral characteristics curve of the synchronous monitoring for agricultural waters and the field surface is shown in Fig. 8. The results of the synchronous monitoring of the water quality in the agricultural waters of the city and the gray value of the ground satellite images are shown in Table 1.

3.2. Results of INSAR image preprocessing

Scene 1 is used to make the comparison test for the image processing of agricultural waters. The scenario is a 6,000 × 6,000 connected area of agricultural waters. Figs. 9(a)–(c) are the results of the INSAR image preprocessing for Scene 1 by using the proposed method, the *K* mean clustering method the local connectivity method, respectively.

In order to verify the robustness of the proposed method, the method is further tested by using the agricultural water Scene 2 with different background [24–26]. The results of the four methods are as shown in Fig. 10, and the agricultural waters in this scene are divided into two non-connected regions by the INSAR. Figs. 10(a)–(d) are the results of the proposed method, the *K* mean clustering method, the local threshold method and the local connectivity method, respectively.

Tables 2 and 3 are the evaluation indexes for the INSAR image preprocessing performance of agricultural waters by using the four methods, respectively.
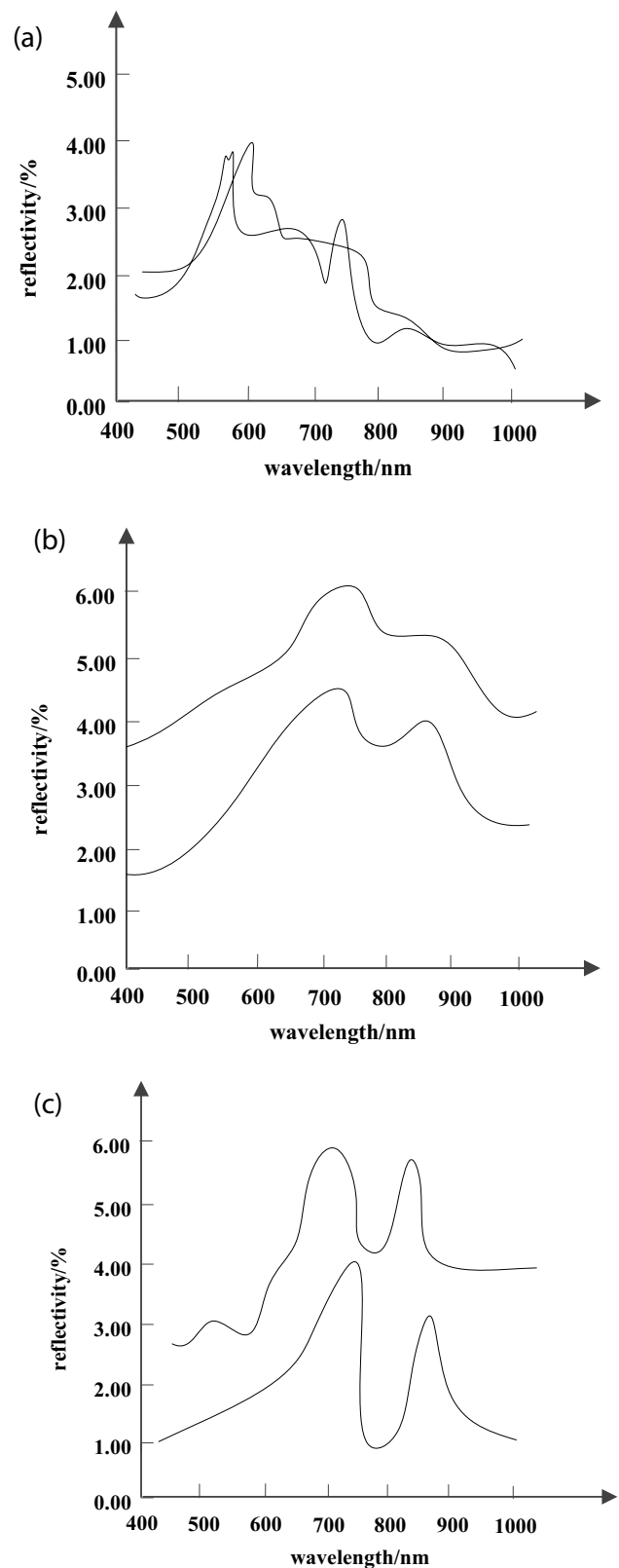

Fig. 8. Pop characteristic curves for simultaneous monitoring of agricultural waters and field surfaces. (a) Reservoir, (b) river, and (c) sewage water body.

Table 1
Synchronous monitoring results of agricultural water quality and gray value of satellite images

(a) Water quality monitoring data

Sampling point		Water quality monitoring and analysis value/(mg L^{-1})				
		SS	Oil	Total phosphorus	COD	Chlorophyll a
A reservoir	HW$_{1-1}$	11	–	0.02	2.87	8.69
	HW$_{1-2}$	13	0.03	0.03	3.16	9.54
	HW$_{1-3}$	17	0.02	0.02	3.00	7.16
	HW$_{1-4}$	10	–	0.03	2.87	15.27
	HW$_{1-5}$	16	–	0.03	3.06	7.21

(b) Gray value of satellite image

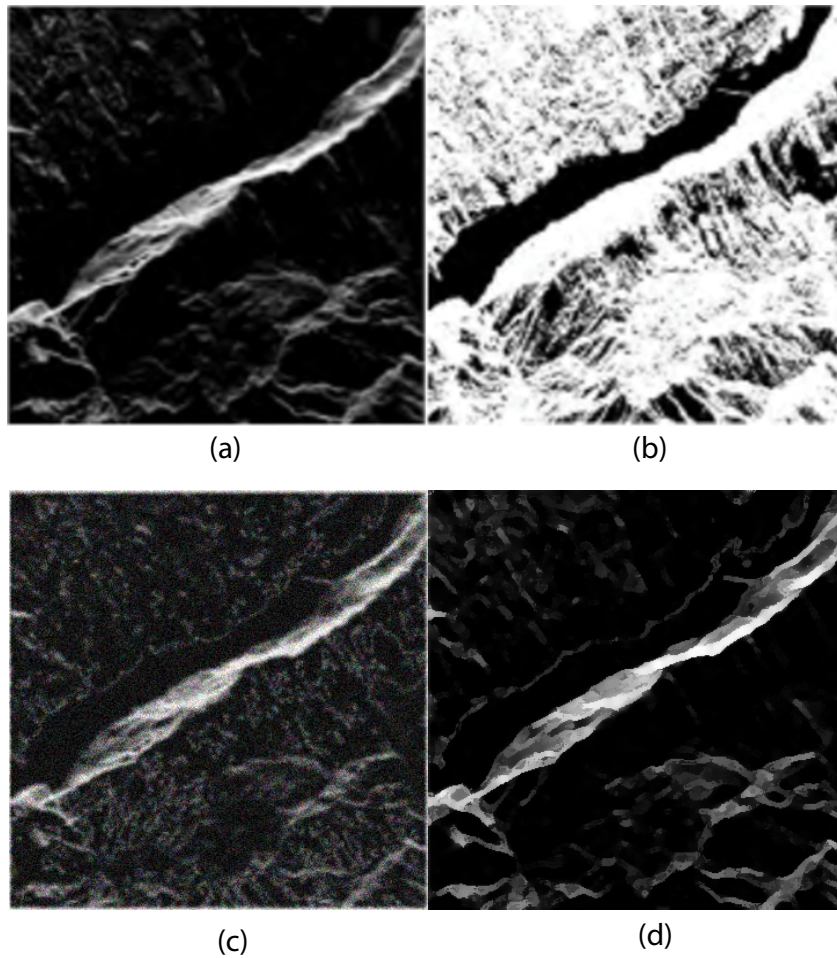| Sampling point		Gray value of satellite image						
		B1	B2	B3	B4	B5	B6	B7
A reservoir	HW	132	57	57	39	24	122	10
	HW	130	58	60	40	24	119	9
	HW	132	58	59	40	25	123	12
	HW	132	58	62	51	25	126	10
	HW	129	57	58	40	24	125	9

Fig. 9. Experimental results of Scene 1. (a) The proposed method, (b) The K mean clustering method, (c) The local threshold method, and (d) The local connectivity method.
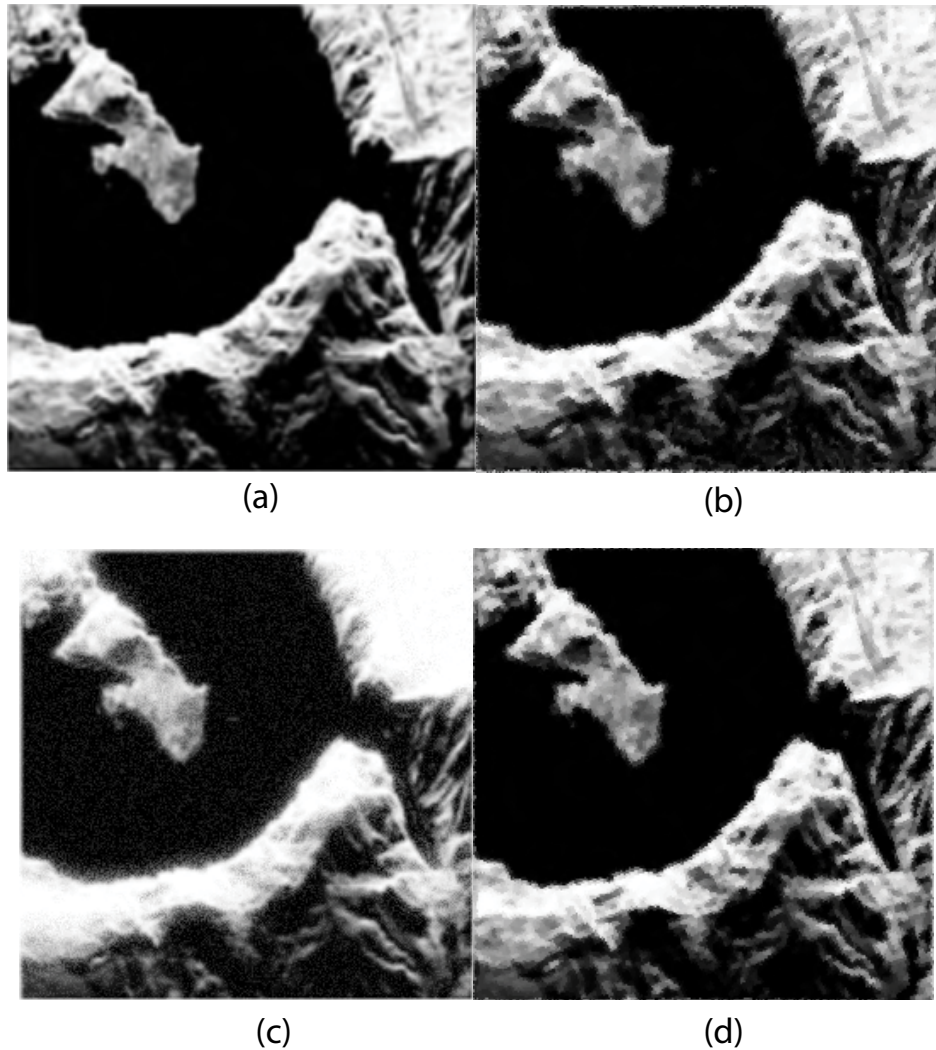
Fig. 10. Experimental results of Scene 2. (a) The proposed method, (b) The K mean clustering method, (c) The local threshold method, and (d) The local connectivity method.

Table 2
Performance index of water extraction in Scene 1

Method	False alarm rate (%)	Leakage rate (%)	Average offset pixel (individual)	Running time (n)
This paper method	0.04	0.02	0.69	387.74
K mean clustering method	0.05	0.66	1.44	1,458.92
Local threshold method	0.08	0.06	2.82	1,675.74
Local connectivity method	1.07	0.41	1.15	2,147.09

Table 3
Performance index of water extraction in Scene 2

Method	False alarm rate (%)	Leakage rate (%)	Average offset pixel (individual)	Running time (n)
This paper method	1.19	3.04	1.28	465.28
K mean clustering method	4.59	7.63	2.37	1,522.07
Local threshold method	2.82	9.31	3.88	1,875.36
Local connectivity method	10.65	6.55	5.29	1,387.94

3.3. Edge feature enhancement of INSAR images

Mathematical morphology is used to enhance the edge features of INSAR image in an agricultural water area, and the results are as shown in Fig. 11(a), and the results of direct edge detection are shown in Fig. 11(b).

3.4. Monitoring results of pollution disaster in agricultural waters

In order to verify the applicability of the proposed method, the validated experiment is carried out with measured data. The monitoring image of agricultural water pollution disaster in a certain area of a province is shown in Fig. 12. The test started in 2016 and ended in 2017. Images were formed during the test. Figs. 12(a) and (b) are the INSAR image before and after the occurrence of the pollution disaster, respectively [27]. Fig. 12(c) is the enhancement area after the occurrence of a pollution disaster relative to before the occurrence, and Fig. 12(d) is the weakened region after the occurrence of a pollution disaster relative to before the occurrence, and they are all gray image [28]. To enhance the display effect, Fig. 12(e) is a pseudo-color display of the monitoring results.

4. Discussion

4.1. Discussion on the results of synchronous monitoring of spectral characteristics

From Fig. 8, we can see that there are two reflection peaks in the wave characteristics curves of the river water and the ground spectrum. The wavelengths are 550–700 and 690–810 nm, respectively. By analyzing the characteristics of

Fig. 11. Comparison of two methods to deal with the results. (a) Mathematical morphology processing results, and (b) direct edge detection results.

the typical spectral curves of the region, the reflectance of the first reflection peak is obviously positively correlated with SS and COD.

There are two reflection peaks in the wave characteristics curves of the water and ground spectrum of the reservoir, which are 550–570 and 680–700 nm, respectively. Through the analysis of the typical spectral curves of the region, the reflectance of the second reflection peaks is positively related to SS, COD, chlorophyll a, and total phosphorus.

There are two reflection peaks in the characteristic curves of the pollutant discharge water and the ground spectrum. The wavelengths are 680–700 and 800–810 nm, respectively. Through the characteristic analysis of the typical spectral curves of the region, the reflectance of the first and second reflection peaks is obviously positively correlated with SS, COD, and petroleum. The results of the synchronous monitoring of agricultural waters in Table 1 show that there is a significant correlation between the water quality and the gray value of the ground satellite images, and the correlation coefficient is about 0.8.

According to the above analysis, there is a regular change between the ground spectral data and the monitoring results of spectral characteristics of agricultural waters. The experimental results show that the pollution disaster in agricultural waters has a significant correlation with the satellite reflection spectrum on the ground. This conclusion has important practical value for monitoring and scheduling of pollution disaster in agricultural waters.

4.2. Discussion on the results of INSAR image preprocessing

As can be seen from Fig. 9, the images of Fig. 9(b) have a lot of false information obviously, the images of Figs. 9(c) and (d) can also clearly see a lot of interference information, and the image clarity is not enough. The image in Fig. 9(a) is preprocessed by the proposed method, and it is obvious that the false areas which are not connected with agricultural waters can be removed almost completely. The gray line in the image is the boundary map of agricultural waters. The extracted water boundary has a good match with the boundary of the actual image, and the image after processing is high and realistic, which greatly improves the quality of pollution monitoring and scheduling in agricultural waters.

From Fig. 10, it can be clearly seen that some shaded parts are separated from agricultural waters and are inaccurate in extracting waters. Apparently, the shadow part of Fig. 10(a) preprocessed by this method is basically removed, the precision of the extraction of water boundary is high, the overall effect of the image is better than the other three methods, which proves the robustness of the proposed method to different scene processing, showing that the proposed method can be applied to the agricultural waters of different scenes, pollution monitoring, and scheduling can be achieved and satisfactory results can be obtained.

Tables 2 and 3 show the quantitative results of four methods for image preprocessing of Scenes 1 and 2. The *K* mean clustering method reduces the false alarm rate by setting multiple thresholds, but it also causes the phenomenon of over segmentation and increases the missing detection rate. The local threshold method does not improve the missing
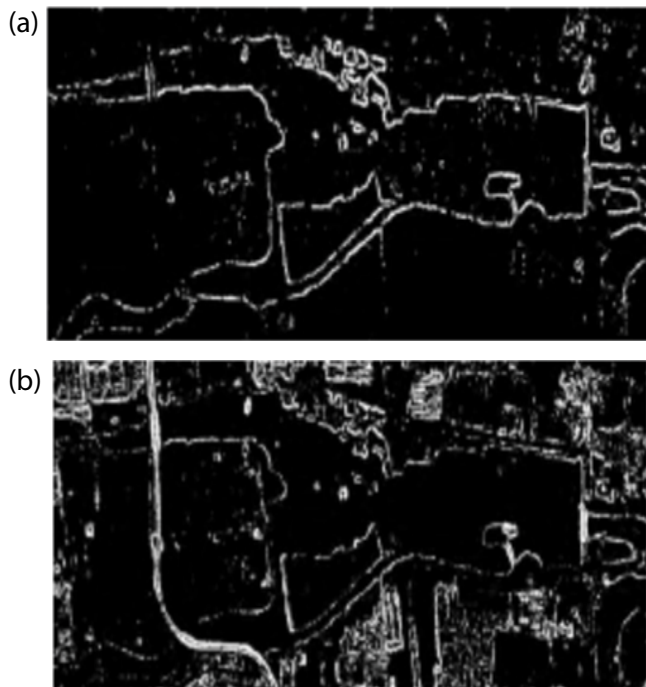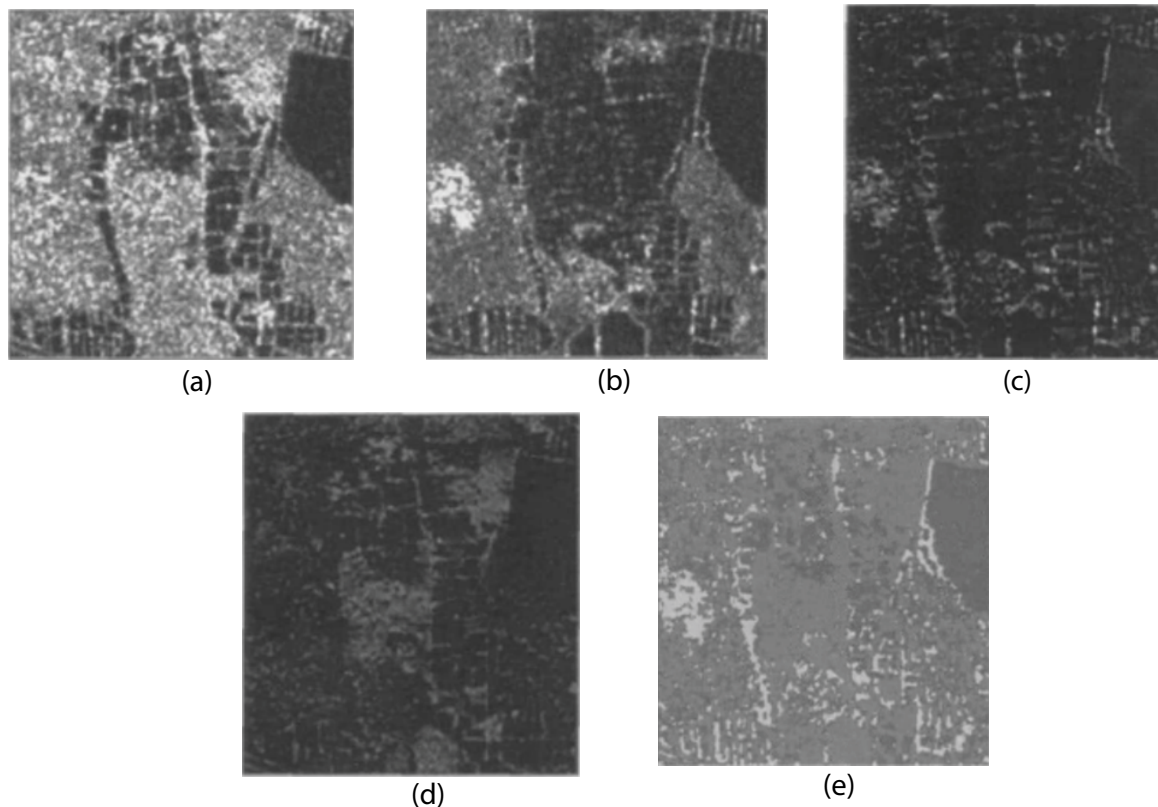
Fig. 12. Monitoring images of pollution damage in agricultural waters of a certain area. (a) Before the occurrence of pollution disasters, (b) After the pollution disaster, (c) Enhanced areas after pollution disasters, (d) Weakened areas after pollution disasters, and (e) Pseudo-color surveillance area image.

detection problem, and the false alarm rate of the local connectivity method is obviously higher. The false alarm rate and missing detection rate of the proposed method are lower in different scenarios, and the contour average deviation of agricultural waters is the lowest, so the contour accuracy is higher. In addition, the operation time of the proposed method is relatively short. When the image is large and the agricultural waters are widely distributed, the method of this paper has significant advantages in the accuracy of INSAR image extraction and operation efficiency.

4.3. Discussion on the results of using mathematical morphology to enhance the edge features of INSAR images

The proposed method is used to enhance the edge features of INSAR images in agricultural waters. As can be seen from Fig. 11, the proposed method can effectively solve the problem of false alarm in water edge detection when there are many objects such as waters and buildings in INSAR image. In this paper, after preprocessing the two-dimensional gray histogram of INSAR image, the edge feature is enhanced by mathematical morphology, and the strong scattering points and speckle noise are suppressed, and the applicable scene of the edge detection algorithm in agricultural waters is expanded. Compared with the result of edge detection without edge feature processing, the proposed method can effectively restrain the edge of the buildings and other objects around the agricultural waters and improve the monitoring

effect of the pollution disaster in agricultural waters based on INSAR.

4.4. Discussion on the results of monitoring results of pollution disaster in agricultural waters

As shown in Fig. 12, when the pollution disaster in agricultural waters did not occur, the area with no stained water covered in the image showed a brighter color, as shown in Fig. 12(a). The scattering mechanism of the object is changed from the original diffuse scattering to the mirror scattering due to the inundation of a large number of areas, which has changed the scattering mechanism from the original diffuse scattering. Therefore, the dark area of the INSAR image is presented, as shown in Fig. 12(b). From Figs. 12(c)–(e), it is known that the INSAR image extracted by the proposed method is distinct, and the information of the pollution disaster change is relatively accurate, which can be used for monitoring and scheduling of the pollution disaster in agricultural waters.

5. Conclusion

In recent years, the development of agricultural waters has increased, resulting in frequent damage to agricultural waters. In this paper, an INSAR-based monitoring and scheduling method for pollution disaster in agricultural waters is proposed, which can conduct comprehensive and accurate

monitoring of pollution disaster in agricultural waters. By preprocessing the two-dimensional gray histogram of INSAR image and enhancing the edge features of INSAR image by mathematical morphology, this method can extract the boundary of agricultural waters based on INSAR accurately, and instead of the common *K* mean clustering method and local threshold method. At the same time, through the analysis of the field ground spectral monitoring specification, it is concluded that there is a correlation between the agricultural water pollution and the ground and the satellite reflection spectrum, and the correlation coefficient of the two is 0.8. This conclusion is helpful to the monitoring and scheduling of the pollution disaster in the agricultural waters. After the INSAR image preprocessing experiment, it is proved that the proposed method has the advantages of low false alarm rate, low leakage detection rate, and high precision of contour processing in different agricultural waters. The results of the pollution disaster monitoring in agricultural waters can be obtained. This method can obtain accurate information on the fluctuation of agricultural water pollution and improve the quality of pollution monitoring and scheduling in agricultural waters.

Acknowledgment

References

[1] D. Chicalote-Castillo, P. Ramirez-Garcia, M.L. Macias-Rubalcava, Allelopathic effects among selected species of phytoplankton and macrophytes, J. Environ. Biol., 38 (2017) 1221–1227.

[2] D. Li, S. Ge, W. Peng, Q. Wu, J. Wu, Chemical structure characteristics of wood/lignin composites during mold pressing, Polym. Compos., 38 (2017) 955–965.

[3] H. Ouyang, K. Hou, L. Wang, W. Peng, Optimization protocol for the microwave-assisted extraction of antioxidant components from pinus elliottii needles using response surface methodology, BioResources, 12 (2017) 478–494.

[4] M. Soares, S. Bianco, E.L. Finoto, D. Bolonhezi, J. Albuquerque, Phytosociological study on the weed communities in green sugarcane field reform using conservation tillage and oilseed crops in succession, Appl. Ecol. Environ. Res., 15 (2017) 417–428.

[5] C.A. Benbow, J.H. MacMahan, E.B. Thornton, Analysis of surface foam holes associated with depth-limited breaking, J. Coastal Res., 33 (2017) 1271–1282.

[6] C. Bo, G. Shelach, Fortified settlements and the settlement system in the northern zone of the Han empire, Antiquity, 88 (2014) 222–240.

[7] J. Sawicki, Magnetohydrodynamic flow of viscous fluid in a slot between fixed surfaces of revolution, Polish Marit. Res., 24 (2017) 78–85.

[8] S. Wu, S. Lin, H. Li, W. Chai, Q. Zhang, Y. Wu, W. Zhu, A study on workplace violence and its effect on quality of life among medical professionals in china, Archives Environ. Occup. Health, 69 (2014) 81–88.

[9] J. Li, X. Li, N. Lv, Quantitative assessment of groundwater pollution intensity on typical contaminated sites in China using grey relational analysis and numerical simulation, Environ. Earth Sci., 74 (2015) 3955–3968.

[10] W. Zhu, Q. Zhang, X.L. Ding, Landslide monitoring by combining of CR-InSAR and GPS techniques, Adv. Space Res., 53 (2014) 430–439.

[11] T.E. Keskin, M. Düğenci, F. Kaçaroğlu, Prediction of water pollution sources using artificial neural networks in the study areas of Sivas, Karabük and Bartın (Turkey), Environ. Earth Sci., 73 (2015) 5333–5347.

[12] S.K. Bhattacharya, A comparison of the predicted vulnerability zones with the data based on hazard zones of landslide in the Kurseong hill subdivision, Darjeeling district, West Bengal, India, Environ. Earth Sci., 75 (2016) 1–10.

[13] H. Yao, T. Zhang, B. Liu, Analysis of surface water pollution accidents in china: characteristics and lessons for risk management, Environ. Manage., 57 (2016) 868–878.

[14] Q.U. Yanping, G. Hui, L. Juan, Agricultural drought disaster risk assessment in China based on the regional disaster system theory, J. Hydraul. Eng., 46 (2015) 908–917.

[15] M. Xie, J. Huang, L. Wang, Early landslide detection based on D-InSAR technique at the Wudongde hydropower reservoir, Environ. Earth Sci., 75 (2016) 1–13.

[16] P. Castellazzi, R. Martel, A. Rivera, Groundwater depletion in Central Mexico: use of GRACE and InSAR to support water resources management, Water Resour. Res., 52 (2016) 5985–6003.

[17] J. Chen, H.A. Zebker, R. Knight, A persistent scatterer interpolation for retrieving accurate ground deformation over InSAR-decorrelated agricultural fields, Geophys. Res. Lett., 42 (2016) 9294–9301.

[18] H.H. Chang, D. Zilberman, On the political economy of allocation of agricultural disaster relief payments: application to Taiwan, Europ. Rev. Agric. Econ., 41 (2014) 169–180.

[19] C. Zhao, B. Chen, Driving force analysis of the agricultural water footprint in China based on the LMDI method, Environ. Sci. Technol., 48 (2014) 12723–12731.

[20] A. Ruiz-Constán, A.M. Ruiz-Armenteros, F. Lamas-Fernández, Multi-temporal InSAR evidence of ground subsidence induced by groundwater withdrawal: the Montellano aquifer (SW Spain), Environ. Earth Sci., 75 (2016) 242.

[21] I. Choudhury, B. Bhattacharya, An assessment of satellite-based agricultural water productivity over the Indian region, Int. J. Remote Sens., 39 (2018) 2294–2311.

[22] J. Martínez-Fernández, A. González-Zamora, N. Sánchez, A soil water-based index as a suitable agricultural drought indicator, J. Hydrol., 522 (2015) 265–273.

[23] A. Prabhakaran, N.J. Raj, Mapping and analysis of tectonic lineaments of Pachamalai hills, Tamil Nadu, India using geospatial technology, Geol. Ecol. Landscapes, 2 (2018) 81–103.

[24] T.D.T. Oyedotun, X-ray fluorescence (XRF) in the investigation of the composition of earth materials: a review and an overview, Geol. Ecol. Landscapes, 2 (2018) 148–154.

[25] J.R.J. Hamad, M.M. Hanafiah, S. Abdullah, Problems and current practices of solid waste management in the city of almarj, Libya, J. CleanWAS, 1 (2017) 1–5.

[26] N. Shahidah, S. Hasnah, S. Shuhaili, A. Syamzany, M.A. Mohd Shukri, Indoor airborne bacteria and fungi at different background area in nurseries and day care centres environments, J. CleanWAS, 1 (2017) 36–39.

[27] A.A. Mahzan, A.S. Ramli, A.S.M. Abduh, I. Izhar, M.Z.M.Y. Indirakumar, A.A.M. Salih, A.S.A. Jahri, O.Q. Wei, Preliminary study of SG serai hot spring, Hulu Langat, Malaysia, Water Conserv. Manage., 1 (2017) 11–14.

[28] B. Andik, A. Sarang, Daylighting Buried Rivers and Streams in Tehran, Water Conserv. Manage., 1 (2017) 1–4.